



OPEN

Ag₂CO₃ containing magnetic nanocomposite as a powerful and recoverable catalyst for Knoevenagel condensation

Fatemeh Karimkhan, Dawood Elhamifar[✉] & Masoumeh Shaker

In this paper, the synthesis, characterization and catalytic application of a novel magnetic silica-supported Ag₂CO₃ (MS/Ag₂CO₃) with core-shell structure are developed. The MS/Ag₂CO₃ nanocomposite was prepared through chemical modification of magnetic MS nanoparticles with AgNO₃ under alkaline conditions. The structure, chemical composition and magnetic properties of MS/Ag₂CO₃ were investigated by using VSM, PXRD, FT-IR, EDX and SEM techniques. The MS/Ag₂CO₃ nanocomposite was used as an effective catalyst for the Knoevenagel condensation under solvent-free conditions at 60 °C in an ultrasonic bath. The recovery and leaching tests were performed to study the nature of the MS/Ag₂CO₃ catalyst under applied conditions.

Magnetic nanoparticles (NPs) have wide applications in various fields of medicine, catalysis, environment, materials science and biotechnology due to their unique magnetic properties and ability to respond to external magnetic fields. Therefore, in recent years, many researchers have focused on making different types of these NPs. The cobalt, iron, nickel elements and their chemical compounds are precursors that commonly used to prepare magnetic NPs^{1–9}. The use of nickel and cobalt is limited due to their toxicity and high tendency to oxidize. Among these, magnetic iron oxide NPs, especially superparamagnetic Fe₃O₄ NPs, have been considered by researchers due to their non-toxicity, good biocompatibility and good magnetic properties^{10,11}. Magnetic NPs, despite having many advantages, suffer from a series of inherent disadvantages such as high chemical activity and a high tendency to aggregate due to their high surface area. Therefore, the development of effective strategies to improve the stability of these NPs is an essential need. Coating the surface of Fe₃O₄ NPs is one of the effective methods to stabilize them. The species including organic polymers such as dextran, chitosan, polyethylene glycol, polyaniline; organic surfactants such as CTAB, DTAB, DPB and SOS; metals such as Au and Ag; mineral oxides such as carbon and silica; biological molecules and structures such as ligands/receptors, peptides, liposomes have been used as coating shell for Fe₃O₄ NPs to form core-shell structured MNPs^{10,12–24}. Some of the recently developed reports in this matter are dextran-coated Fe₃O₄ MNPs¹², Fe₃O₄/chitosan¹³, Fe₃O₄/CTAB¹⁷, Fe₃O₄/Au_nAc-FA NCPs¹⁸, Fe₃O₄@Ag¹⁹, Fe₃O₄@C²⁰, Fe₃O₄-OS-SO₃H¹⁰ and DOX-Fe₃O₄-TSL²⁴. Among the various protective shells, silica has attracted more attention between many researchers. The silica shell can reduce the magnetic dipole adsorption between nanoparticles, helping to diffuse magnetic NPs in aqueous and organic environments. Also due to poor chemical permeability, silica can prevent the destruction of MNPs in different chemical environments. Moreover, the abundant silanol groups on the silica surface provide suitable conditions for different types of modification^{10,25–28}. Some of recently developed magnetic nanostructures with silica shells are Fe₃O₄@BOS@SB/In²⁹, Fe₃O₄@SiO₂@PMO³⁰, Re-SiO₂-Fe₃O₄³¹, Mag@Ti-NOS³², Fe₃O₄@RF@void@PMO(IL)/Cu³³, Fe₃O₄@SiO₂@propyl-ANDSA³⁴ and Fe₃O₄@Au@mSiO₂-dsDNA/DOX³⁵. The MNPs with silica shell can be used as electrode³⁶, adsorbent³⁷, sensor³⁸, catalyst support^{10,29,32–34,39,40}, ion exchanger⁴¹ and so on. Especially, in the field of catalysis, magnetic silicas with a core-shell structure have been considered by many researchers due to their magnetic recoverability, high hydrophobicity and ability to modify their surface^{42–46}. Some of recently developed nanocatalysts are Fe₃O₄@SiO₂/Schiff-base/Cu(II)⁴², Fe₃O₄@SiO₂-EDTA-Ni⁴³, Fe₃O₄@SiO₂-IL⁴⁴, Fe₃O₄@SiO₂/Ru-WO_x⁴⁵ and IL-Fe₃O₄@SiO₂⁴⁶.

Transition metal catalysts have been useful in modern synthetic organic chemistry due to their diverse reactivity in enabling various molecular conversions⁴⁷. The reactions performed using these catalysts can be classified into three groups based on the role of the metal: 1. catalytic reactions based on the oxidation/reduction cycle of the transition metal, 2. catalytic reactions in which the transition metal acts as a Lewis acid and 3.

Department of Chemistry, Yasouj University, 75918-74831 Yasouj, Iran. ✉email: d.elhamifar@yu.ac.ir

reactions catalyzed by coinage metals (Cu, Ag and Au)⁴⁸. In recent years, silver metal has been more considered by researchers as an effective transition metal catalyst, due to the processes catalyzed by silver perform under mild conditions and silver is cheaper and environmentally friendly than many rare metals (Pd, Pt, Rh, Ru, etc.). Among the various silver species, silver carbonate (Ag_2CO_3) can be employed as a Lewis acid, an inorganic base and a good oxidant in different organic reactions. Also, Ag_2CO_3 can be coordinated with various unsaturated systems (carbonyls, imines, isocyanides, alkynes and alkenes) and create very stable intermediates in the course of various processes^{48–53}.

On the other hand, the Knoevenagel condensation of active methylene and carbonyl compounds is among the most commonly used methods in organic chemistry for the synthesis of low-electron olefins. In recent years, many catalysts were used for Knoevenagel condensation, in which heterogeneous ones have received much attention due to the easy recovery of the catalyst and also the easy separation of the products^{54–61}. Some of the recently reported heterogeneous catalytic systems are $\text{Fe}_3\text{O}_4@OS\text{-NH}_2$ ⁵⁴, CAU-1- NH_2 ⁵⁵, $\text{MgO}_{S_{400}}$ ⁵⁶, PMO-IL- NH_2 ⁵⁷, IL- H_2O -DABCO⁵⁸, MgO/ZrO_2 ⁵⁹, CoFe_2O_4 ⁶⁰ and LDH-ILs-C12⁶¹. In view of the above, especially the advantages mentioned for Ag_2CO_3 , our motivation in this study is the design and preparation of a novel core-shell structured MS/ Ag_2CO_3 nanocomposite as a powerful, effective, recyclable and reusable nanocatalyst for the Knoevenagel condensation.

Experimental section

Preparation of MS/ Ag_2CO_3 . For this, the Fe_3O_4 NPs (0.6 g)²⁹ were dispersed in deionized water (25 mL) and EtOH (75 mL) for 0.5 h. After adding NH_3 (3.5 mL, 25% wt), the mixture was stirred at RT for 20 min. Then, tetramethoxysilane (TMOS, 0.5 mL) was added and stirring was continued at RT for 16 h. After that, the resulting solid material was magnetically collected, washed with deionized water and EtOH, dried at 80 °C for 6 h and defined as MS. For preparation of MS/ Ag_2CO_3 , MS (0.6 g) was well-dispersed in deionized water (30 mL). After 0.5 h, NaHCO_3 (2.5 mmol) was added and stirring was continued at RT for 2 h. Then, AgNO_3 (5 mmol) was added under lightless conditions. After that, the reaction combination was stirred for 12 h in an ice bath. The resulted material was collected using a magnetic field, washed with deionized water, dried and designated as MS/ Ag_2CO_3 .

Procedure for the Knoevenagel reaction using MS/ Ag_2CO_3 . For this, MS/ Ag_2CO_3 (0.015 g), ethyl cyanoacetate (1 mmol) and aldehyde (1 mmol) were added in a reaction flask and the resulted mixture was sonicated at 60 °C under solvent-free conditions. After completing of the process, EtOH (10 mL) was added and MS/ Ag_2CO_3 was magnetically separated. Finally, the solvent was evaporated and pure Knoevenagel products were resulted after recrystallization in EtOH and n-hexane solvents.

IR, ^1H NMR and ^{13}C NMR data of Knoevenagel products. (*E*)-ethyl 2-cyano-3-(2-nitrophenyl)acrylate (Table 2, entry 2). Pale yellow solid; yield: 95%; M.P.: 98–100 °C (ref: 102 °C⁶²), IR (KBr, cm^{-1}): 3097 (=C–H, stretching vibration sp^2), 2989 (C–H, stretching vibration sp^3), 2221 (CN, stretching vibration), 1723 (C=O, stretching vibration), 1565, 1462 (C=C, Ar stretching sp^2), 1264 (C–O, stretching vibration), 1529, 1358 (NO_2 , stretching vibration). ^1H NMR (300 MHz, DMSO): δ (ppm) 1.34 (t, 3H, $J=6.0$ Hz), 4.38 (q, 2H), 7.84–7.89 (m, 1H), 7.93–8.02 (m, 2H), 8.33 (d, 1H, $J=9.0$ Hz), 8.86 (s, 1H). ^{13}C NMR (75 MHz, DMSO): δ (ppm) 14.4, 63.1, 107.8, 114.7, 125.7, 128.7, 131.0, 132.9, 135.2, 147.7, 155.6, 161.4.

(*E*)-ethyl 2-cyano-3-(4-nitrophenyl)acrylate (Table 2, entry 3). Pale yellow solid; yield: 97%; M. P.: 170–171 °C (ref: 168 °C⁶³), IR (KBr, cm^{-1}): 3095 (=C–H, stretching vibration sp^2), 2990 (C–H, stretching vibration sp^3), 2226 (CN, stretching vibration), 1718 (C=O, stretching vibration), 1593, 1469 (C=C, Ar stretching sp^2), 1259 (C–O, stretching vibration), 1510, 1350 (NO_2 , stretching vibration). ^1H NMR (300 MHz, DMSO): δ (ppm) 1.31 (t, 3H, $J=6.9$ Hz), 4.33 (q, 2H), 7.82 (d, 2H, $J=13.2$ Hz), 8.00 (d, 2H, $J=10.80$ Hz), 8.40 (s, 1H). ^{13}C NMR (75 MHz, DMSO): δ (ppm) 14.4, 62.9, 103.7, 115.8, 127.7, 131.0, 132.9, 133.0, 154.3, 162.1.

(*E*)-ethyl 3-(2-chlorophenyl)-2-cyanoacrylate (Table 2, entry 4). White solid; yield: 92%; M.P.: 52–54 °C (ref: 52–54 °C⁶⁴), IR (KBr, cm^{-1}): 3072 (=C–H, stretching vibration sp^2), 2955 (C–H, stretching vibration sp^3), 2229 (CN, stretching vibration), 1718 (C=O, stretching vibration), 1619, 1475 (C=C, Ar stretching sp^2), 1264 (C–O, stretching vibration). ^1H NMR (400 MHz, CDCl_3): δ (ppm) 1.43 (t, 3H, $J=7.2$ Hz), 4.43 (q, 2H), 7.40–7.47 (m, 1H), 7.50–7.55 (m, 2H), 8.24 (d of d, 1H, $J_1=4.6$ Hz, $J_2=1.6$ Hz), 8.71 (s, 1H). ^{13}C NMR (100 MHz, CDCl_3): δ (ppm) 14.2, 62.9, 106.2, 114.8, 127.5, 129.8, 129.9, 130.3, 133.7, 136.4, 151.1, 161.8.

(*E*)-ethyl 2-cyano-3-(*p*-tolyl)acrylate (Table 2, entry 7). White solid; yield: 91%; M.P.: 95–97 °C (ref: 93–94 °C⁶³), IR (KBr, cm^{-1}): 3025 (=C–H, stretching vibration sp^2), 2961 (C–H, stretching vibration sp^3), 2217 (CN, stretching vibration), 1725 (C=O, stretching vibration), 1604, 1515 (C=C, Ar stretching sp^2), 1261 (C–O, stretching vibration). ^1H NMR (400 MHz, CDCl_3): δ (ppm) 1.42 (t, 3H, $J=7.2$ Hz), 2.46 (s, 3H), 4.42 (q, 2H), 7.33 (d, 2H, $J=8.4$ Hz), 7.93 (d, 2H, $J=8.4$ Hz), 8.25 (s, 1H). ^{13}C NMR (100 MHz, CDCl_3): δ (ppm) 14.2, 22.0, 62.6, 101.5, 115.8, 128.8, 130.1, 131.3, 144.7, 155.0, 162.8.

Results and discussion

The synthesis of MS/ Ag_2CO_3 is shown in Fig. 1. Firstly, the Fe_3O_4 NPs were modified with a silica shell to give MS NPs. Then, the MS NPs were treated with NaHCO_3 and AgNO_3 to deliver the desired MS/ Ag_2CO_3 nanocomposite.

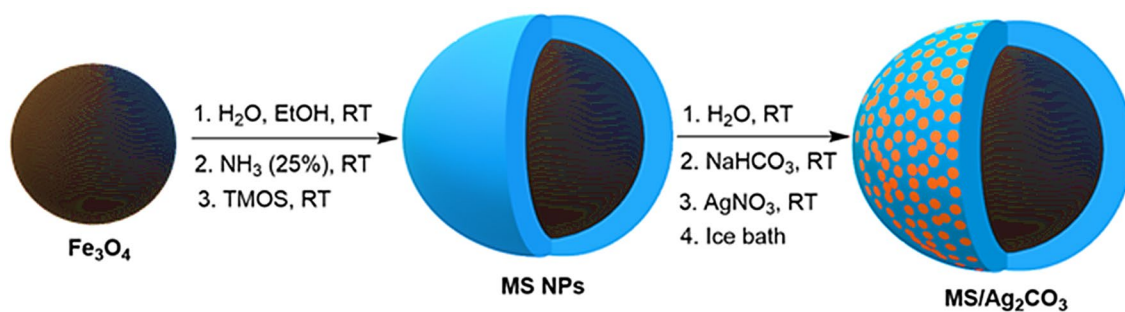


Figure 1. Preparation of the MS/Ag₂CO₃ nanocomposite.

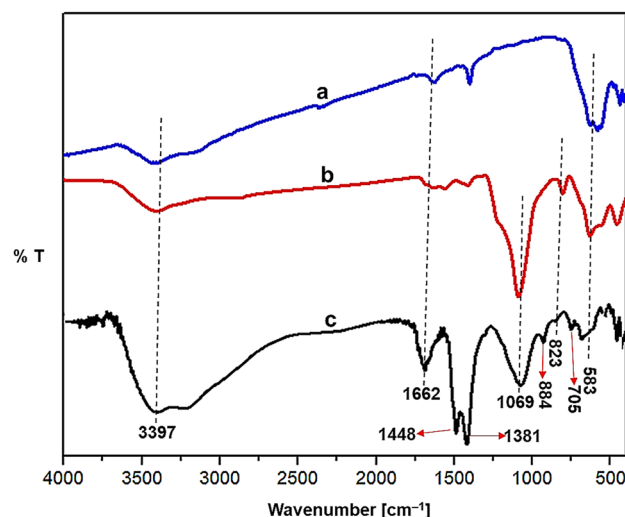


Figure 2. FT-IR of (a) Fe₃O₄, (b) MS and (c) MS/Ag₂CO₃.

The FT-IR spectra of Fe₃O₄, MS and MS/Ag₂CO₃ are shown in Fig. 2. For all samples, the characteristic signals at 3397 and 583 cm⁻¹ are, respectively, due to O–H and Fe–O bonds. Also, the band cleared at 1662 cm⁻¹ is due to bending vibration of O–H bonds^{32,65}. For MS and MS/Ag₂CO₃, the signals at 823 and 1069 cm⁻¹ are assigned to Si–O–Si, confirming the construction of SiO₂ shell around the Fe₃O₄ core (Fig. 2b,c)²⁶. Importantly, for the MS/Ag₂CO₃ nanocomposite, the observed peaks at 705, 884, 1381 and 1448 cm⁻¹ are attributed to the absorption bands of CO₃²⁻ (Fig. 2c), indicating successful immobilization of Ag₂CO₃ particles on the surface of MS⁶⁶.

The wide-angle PXRD pattern of Fe₃O₄ and MS/Ag₂CO₃ nanomaterials are shown in Fig. 3. As shown, for both samples, six characteristic peaks are observed at 2θ of 30.10, 35.58, 43.29, 53.81, 57.44 and 63.24 degree, corresponding to the crystal planes of (220), (311), (400), (422), (511) and (440), respectively. These are related to the crystalline structure of magnetite NPs confirming high stability of Fe₃O₄ during catalyst preparation. The pattern of MS/Ag₂CO₃ nanocomposite also showed two sharp peaks at 2θ of 33.2 and 38.5 degree corresponding to the Ag₂CO₃ NPs (Fig. 3b)^{10,66,67}. This proves successful construction of Ag₂CO₃ NPs on MS core.

The VSM analysis was done to investigate the magnetic property of MS/Ag₂CO₃ nanocomposite (Fig. 4). As shown, the saturation magnetization of 17.5 emu/g was found for this material. Also, the VSM curve showed that this material has a superparamagnetic behavior.

The surface morphology of MS/Ag₂CO₃ nanocomposite was studied by using SEM analysis. This showed that the MS/Ag₂CO₃ nanocomposite has a uniform spherical structure (Fig. 5).

The EDX spectrum showed that the designed MS/Ag₂CO₃ is composed of Fe, Si, O, Ag and C elements confirming the successful incorporation/immobilization of expected species in the material framework (Fig. 6).

In the following, the catalytic activity of MS/Ag₂CO₃ was evaluated in the Knoevenagel reaction. To obtain the optimum conditions, the reaction of benzaldehyde with ethyl cyanoacetate was chosen as a model (Table 1). The study showed that the catalyst loading is a very important factor in the reaction progress, in which the best result was obtained using 0.015 g of catalyst (Table 1, entries 1–4). The solvent screening demonstrated that solvent-free condition is the best for the reaction (Table 1, entries 4–8). Evaluation of temperature showed that the highest activity of MS/Ag₂CO₃ is resulted at 60 °C (Table 1, entry 4 *versus* entries 9, 10). In the next, the activity of Ag₂CO₃-free Fe₃O₄ and MS nanomaterials was compared with that of MS/Ag₂CO₃ showing that the presence of Ag₂CO₃ particles as active catalytic centers are necessary for the development of the reaction (Table 1, entry 4 *versus* entries 11, 12). To prove the effect of both Ag and CO₃ species in the reaction progress, the catalytic activity of MS/Ag₂CO₃ was compared with AgCl, Na₂CO₃ and NaNO₃ salts (Table 1, entry 4 *versus* entries 13–15). The

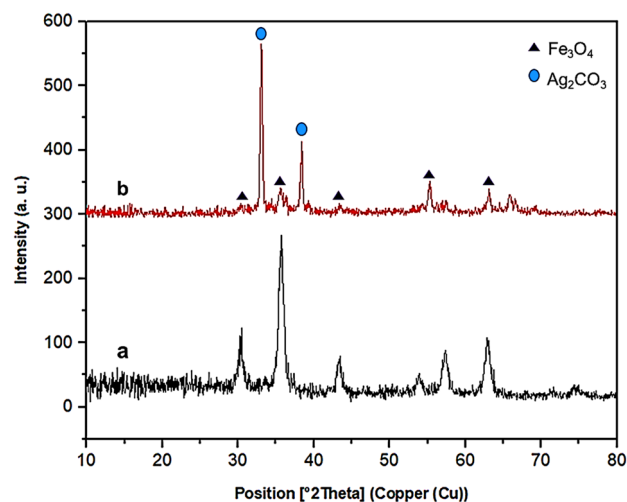


Figure 3. Wide angle-PXRD pattern of the (a) Fe_3O_4 and (b) $\text{MS}/\text{Ag}_2\text{CO}_3$ nanomaterials.

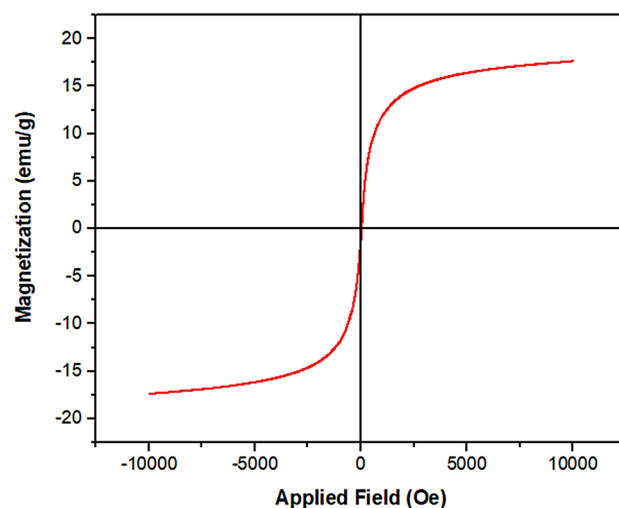


Figure 4. VSM of the $\text{MS}/\text{Ag}_2\text{CO}_3$.

results showed that AgCl and Na_2CO_3 deliver a low to moderate yield of desired product. While, using NaNO_3 , no progress was observed in the reaction. Interestingly, in the presence of designed $\text{MS}/\text{Ag}_2\text{CO}_3$ the best result was obtained. These confirm that both Ag and CO_3 species are necessary for the development of reaction. According to these results, it can be concluded that the designed $\text{MS}/\text{Ag}_2\text{CO}_3$ acts as a bifunctional catalyst in the reaction.

With the optimal conditions in hand that are bolded in Table 1 (entry 4), a variety of aldehydes were employed as substrate (Table 2). Generally, for aromatic aldehydes bearing both electron-withdrawing or electron-donating substituents, electronic nature or substitution pattern had little effect on this process and $\text{MS}/\text{Ag}_2\text{CO}_3$ was able to effectively catalyze the reaction to give the Knoevenagel products in high to excellent yields. Also, terephthalaldehyde, hetero-aromatic aldehydes such as thiophene-2-carbaldehyde and furan-2-carbaldehyde, 1-naphthaldehyde and hexanal also gave the corresponding Knoevenagel adducts in good to high yield at relatively short time. It is important to note that, as previously summarized by Tietze et al., all condensations of cyanoacetate with aromatic and aliphatic aldehydes give E-isomer almost exclusively⁶⁸. In the present study, all synthesized Knoevenagel products were identified as E-isomer by comparing their melting points, IR, and NMR spectra with valid samples^{62–64,69–72}.

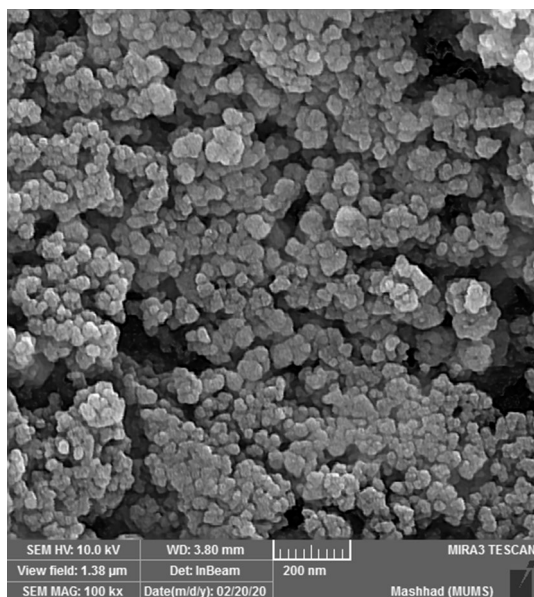


Figure 5. SEM image of MS/Ag₂CO₃.

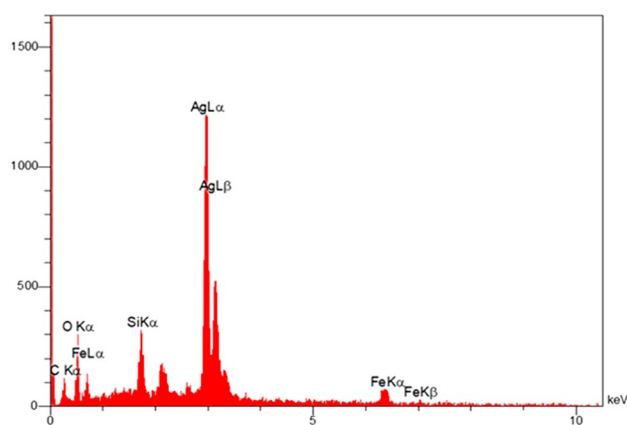
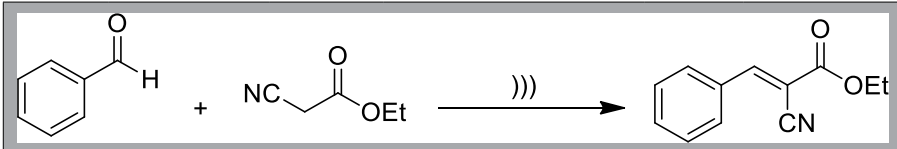


Figure 6. EDX of MS/Ag₂CO₃ nanocomposite.

The ability to recycle and reuse of catalysts are important issues that should be considered in heterogeneous catalytic systems. In this regard, the recyclability and reusability of MS/Ag₂CO₃ catalyst were evaluated in the condensation of benzaldehyde with ethyl cyanoacetate as a test model. For this, in the end of reaction, the catalyst was magnetically separated and reused in the next reaction run at conditions the same as first run. As it is clear in Fig. 7, MS/Ag₂CO₃ can be recovered and reused at least 6 times without the significant loss in its activity and productivity.

For determining the nature of the MS/Ag₂CO₃ catalyst, a leaching test was done at optimal conditions. For this, after progress of about 50% of the process, the MS/Ag₂CO₃ catalyst was collected using a magnet and the reaction progress of the catalyst-free residue was monitored. Importantly, after 1 h, no progress was observed in converting the starting material to product. This proves the heterogeneous nature of the MS/Ag₂CO₃ catalyst and also confirms no-leaching of active Ag₂CO₃ particles during the applied conditions.

Although the exact reaction pathway for the Knoevenagel condensation with the MS/Ag₂CO₃ catalyst is not clear for us, however, based on the results presented for the Ag₂CO₃ catalyst in other organic reactions, a plausible mechanism for this reaction is presented in Fig. 8. Since Ag₂CO₃ has a dual role as a base and a one-electron



Entry	Catalyst	Cat. (g)	Solvent	T (°C)	Yield (%) ^a
1	–	–	Solvent-free	60	–
2	MS/Ag ₂ CO ₃	0.005	Solvent-free	60	78
3	MS/Ag ₂ CO ₃	0.01	Solvent-free	60	85
4	MS/Ag ₂ CO ₃	0.015	Solvent-free	60	96
5	MS/Ag ₂ CO ₃	0.015	Toluene	60	68
6	MS/Ag ₂ CO ₃	0.015	EtOH/Toluene (50:50)	60	75
7	MS/Ag ₂ CO ₃	0.015	EtOH	60	82
8	MS/Ag ₂ CO ₃	0.015	H ₂ O	60	84
9	MS/Ag ₂ CO ₃	0.015	Solvent-free	45	81
10	MS/Ag ₂ CO ₃	0.015	Solvent-free	75	96
11	Fe ₃ O ₄	0.015	Solvent-free	60	34
12	MS	0.015	Solvent-free	60	–
13	Na ₂ CO ₃	0.015	Solvent-free	60	43
14	AgCl	0.015	Solvent-free	60	27
15	NaNO ₃	0.015	Solvent-free	60	–

Table 1. The effect of catalyst, solvent and temperature in the Knoevenagel condensation. ^aReaction condition: benzaldehyde (1 mmol) and ethyl cyanoacetate (1 mmol) under ultrasonic waves for 20 min. ^bIsolated yields.

oxidant⁴⁸, it picks up one acidic proton from the active methylene group of ethyl cyanoacetate to give radical intermediate **1**. Simultaneously, Ag₂CO₃ coordinates to an aldehyde to generate complex **2**. Then, the intermediate **1** is coupled with complex **2** to give radical intermediate **3**. In the next step, radical intermediate **3** provides β-hydroxyl compound **4** by picking up a H atom from the produced AgHCO₃ during the one-electron oxidation. Finally, the desired Knoevenagel product **5** is resulted after dehydration of the β-hydroxyl compound.

At the end, the performance of the MS/Ag₂CO₃ catalyst was compared with the previous catalysts in the Knoevenagel condensation (Table 3). As demonstrated, the study showed that MS/Ag₂CO₃ is a catalyst with higher efficiency, stability and durability time than other catalysts. These findings are attributed to the magnetic nature and the chemically immobilized Ag₂CO₃ particles. In fact, the high performance of Ag₂CO₃ NPs in the catalytic processes is due to its bifunctional role as both inorganic base and Lewis acid.

Conclusion

In summary, a novel magnetic silica-supported Ag₂CO₃ (MS/Ag₂CO₃) was successfully prepared and its catalytic performance was studied. The FT-IR and EDX techniques showed the well immobilization of Ag₂CO₃ particles on the MS nanomaterial. The wide-angle PXRD analysis demonstrated the high stability of Fe₃O₄ NPs during steps of catalyst preparation. The PXRD pattern also confirmed the well formation of Ag₂CO₃ NPs on the MS nanocomposite. The superparamagnetic behavior of MS/Ag₂CO₃ was confirmed by the VSM analysis. The SEM image also demonstrated a uniform spherical structure for this catalyst. The MS/Ag₂CO₃ nanocatalyst was efficiently employed in the Knoevenagel condensation under moderate conditions and delivered the desired products in high to excellent yield. Also, MS/Ag₂CO₃ could be recycled and reused with maintaining its activity in several times.

Entry	Aldehyde	Time (min)	Yield (%) ^a	Found M. P. (°C)	Reported M. P. (°C)
1		20	96	51–53	50–51 ⁶²
2		20	95	98–100	102 ⁶²
3		15	97	170–171	168 ⁶³
4		25	92	52–54	52–54 ⁶⁴
5		18	94	87–89	87–89 ⁶²
6		15	96	88–90	90–91 ⁷⁰
7		25	91	95–96	93–94 ⁶²
8		30	88	170–171	169 ⁶²
9 ^b		20	91	198–200	200 ⁷¹
10		20	93	85–87	85–87 ⁶⁴
11		22	92	95–97	95–96 ⁷²
12		20	94	82–84	81–82 ⁷¹
13		30	83	Colorless oil	Colorless oil ⁶⁴

Table 2. Preparation of the Knoevenagel products using MS/Ag₂CO₃. ^aIsolated yields. ^bEthyl cyanoacetate (2 mmol).

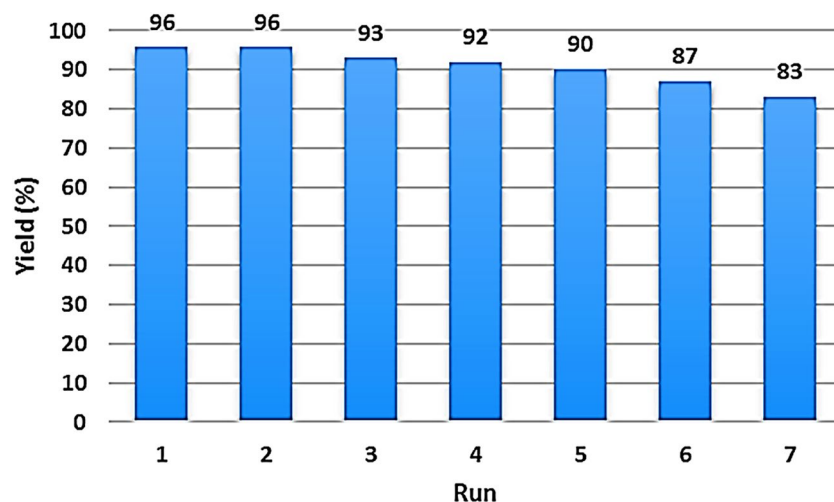


Figure 7. Reusability of the MS/Ag₂CO₃ nanocatalyst.

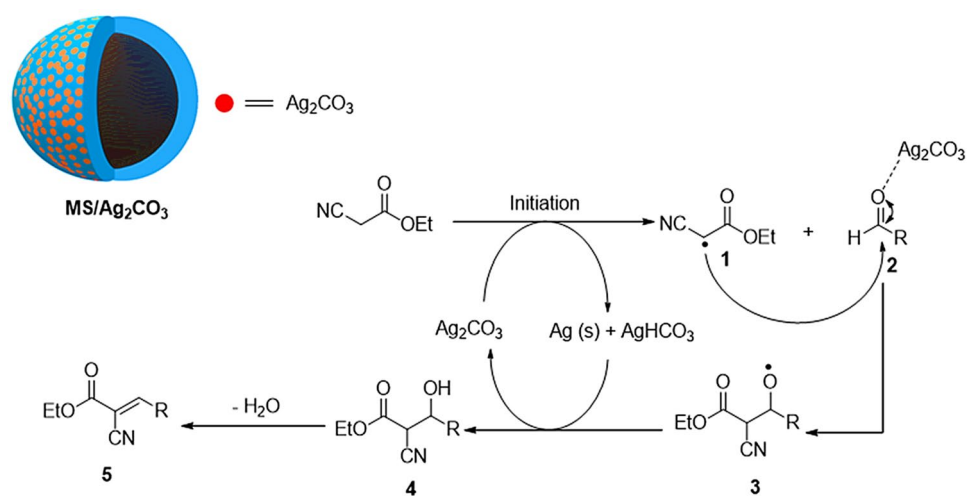


Figure 8. Proposed mechanism for the Knoevenagel condensation using the MS/Ag₂CO₃ catalyst.

Catalyst	Conditions	Recovery times	Refs
FeNPs/PPD@rGO	Cat. 0.05 g, Toluene, 40 °C, 3.5 h	6	⁷³
Y ₂ ZnO ₄	Cat. 0.0136 g, solvent-free, under MW (420 W), 15 min	3	⁷⁴
CoFe ₂ O ₄	Cat. 0.01 g, water/ethanol, 50 °C, 20 min	4	⁶⁰
Zn-MOF	Cat. 0.0693 g, toluene, 50 °C, 48 h	4	⁷⁵
Mg-ABDC	Cat. 0.045 g, ethanol, 80 °C, 7 h	5	⁷⁶
Mg@PS-anthra	Cat. 0.05 g, solvent-free, r. t., 2 h	5	⁷⁷
MS/Ag ₂ CO ₃	Cat. 0.015 g, solvent-free, 60 °C, 20 min,)))	6	This work

Table 3. Comparison of the catalytic activity of MS/Ag₂CO₃ with other catalysts. *PPD* p-phenylenediamine, *rGO* reduced graphene oxide, *MOF* metal-organic framework, *ABDC* 2-aminobenzene-1,4-dicarboxylate anion, *PS* polystyrene, *anthra* anthranilic acid.

Received: 15 March 2021; Accepted: 30 August 2021

Published online: 21 September 2021

References

- Amiri, S. & Shokrollahi, H. The role of cobalt ferrite magnetic nanoparticles in medical science. *Mater. Sci. Eng. C* **33**, 1–8 (2013).
- Fang, C. & Zhang, M. Multifunctional magnetic nanoparticles for medical imaging applications. *J. Mater. Chem.* **19**, 6258–6266 (2009).
- Pourjavadi, A., Hosseini, S. H., Doulabi, M., Fakoorpoor, S. M. & Seidi, F. Multi-layer functionalized poly (ionic liquid) coated magnetic nanoparticles: Highly recoverable and magnetically separable Brønsted acid catalyst. *ACS Catal.* **2**, 1259–1266 (2012).
- Jiang, B. *et al.* Advances of magnetic nanoparticles in environmental application: Environmental remediation and (bio) sensors as case studies. *Environ. Sci. Pollut. Res.* **25**, 30863–30879 (2018).
- Akbarzadeh, A., Samiei, M. & Davaran, S. Magnetic nanoparticles: Preparation, physical properties, and applications in biomedicine. *Nanoscale Res. Lett.* **7**, 144 (2012).
- Colombo, M. *et al.* Biological applications of magnetic nanoparticles. *Chem. Soc. Rev.* **41**, 4306–4334 (2012).
- Reiss, G. *et al.* Magnetoresistive sensors and magnetic nanoparticles for biotechnology. *J. Mater. Res.* **20**, 3294–3302 (2005).
- Bao, Y., Wen, T., Samia, A. C. S., Khandhar, A. & Krishnan, K. M. Magnetic nanoparticles: Material engineering and emerging applications in lithography and biomedicine. *J. Mater. Sci.* **51**, 513–553 (2016).
- Pereira, C. *et al.* Superparamagnetic MFe₂O₄ (M = Fe, Co, Mn) nanoparticles: Tuning the particle size and magnetic properties through a novel one-step coprecipitation route. *Chem. Mater.* **24**, 1496–1504 (2012).
- Shaker, M. & Elhamifar, D. Sulfonic acid supported on magnetic methylene-based organosilica as an efficient and recyclable nanocatalyst for biodiesel production via esterification. *Front. Energy Res.* **8**, 78 (2020).
- Kargar, S., Elhamifar, D. & Zarnegaryan, A. Core-shell structured Fe₃O₄@ SiO₂-supported IL/[Mo₆O₁₉]: A novel and magnetically recoverable nanocatalyst for the preparation of biologically active dihydropyrimidinones. *J. Phys. Chem. Solids* **146**, 109601 (2020).
- Hong, R. *et al.* Synthesis, characterization and MRI application of dextran-coated Fe₃O₄ magnetic nanoparticles. *Biochem. Eng. J.* **42**, 290–300 (2008).
- Arias, J. L., Reddy, L. H. & Couvreur, P. Fe₃O₄/chitosan nanocomposite for magnetic drug targeting to cancer. *J. Mater. Chem.* **22**, 7622–7632 (2012).
- Yang, X., Yang, K., Wu, L., Yang, J. & He, Y. Fe₃O₄ nanoparticles functionalized with poly (ethylene glycol) for the selective separation and enrichment of Au (iii). *New J. Chem.* **44**, 1313–1319 (2020).
- Zhang, B. *et al.* Microwave absorption enhancement of Fe₃O₄/polyaniline core/shell hybrid microspheres with controlled shell thickness. *J. Appl. Polym. Sci.* **130**, 1909–1916 (2013).
- Silva, V., Andrade, P., Silva, M., Valladares, L. D. L. S. & Aguiar, J. A. Synthesis and characterization of Fe₃O₄ nanoparticles coated with fucan polysaccharides. *J. Magn. Magn. Mater.* **343**, 138–143 (2013).
- Cherkashina, K., Voznesenskiy, M., Osmolovskaya, O., Vakh, C. & Bulatov, A. Effect of surfactant coating of Fe₃O₄ nanoparticles on magnetic dispersive micro-solid phase extraction of tetracyclines from human serum. *Talanta* **214**, 120861 (2020).
- Cai, H. *et al.* Dendrimer-assisted formation of Fe₃O₄/Au nanocomposite particles for targeted dual mode CT/MR imaging of tumors. *Small* **11**, 4584–4593 (2015).
- Guo, Z. *et al.* Facile strategy for electrochemical analysis of hydrogen peroxide based on multifunctional Fe₃O₄@ Ag nanocomposites. *ACS Appl. Biol. Mater.* **1**, 367–373 (2018).
- Chen, Z. *et al.* Synthesis of amine-functionalized Fe₃O₄@ C nanoparticles for lipase immobilization. *J. Mater. Chem. A* **2**, 18339–18344 (2014).
- Chatterjee, S., Li, X. S., Liang, F. & Yang, Y. W. Design of multifunctional fluorescent hybrid materials based on SiO₂ materials and core-shell Fe₃O₄@ SiO₂ nanoparticles for metal ion sensing. *Small* **15**, 1904569 (2019).
- Bohara, R. A., Thorat, N. D. & Pawar, S. H. Role of functionalization: Strategies to explore potential nano-bio applications of magnetic nanoparticles. *RSC Adv.* **6**, 43989–44012 (2016).
- Kudr, J. *et al.* Magnetic nanoparticles: From design and synthesis to real world applications. *Nanomaterials* **7**, 243 (2017).
- Shen, S. *et al.* Magnetic liposomes for light-sensitive drug delivery and combined photothermal-chemotherapy of tumors. *J. Mater. Chem. B* **7**, 1096–1106 (2019).
- Uskokovic, V. Earthlike and its discontents: A historical critical review of iron (oxide) particles singly and doubly shelled with silica and/or carbon. *ACS Earth Space Chem.* **4**, 1843–1877 (2020).
- Shaker, M. & Elhamifar, D. Magnetic methylene-based mesoporous organosilica composite-supported IL/Pd: A powerful and highly recoverable catalyst for oxidative coupling of phenols and naphthols. *Mater. Today Chem.* **18**, 100377 (2020).
- Liu, J., Qiao, S. Z., Hu, Q. H. & Lu, G. Q. Magnetic nanocomposites with mesoporous structures: Synthesis and applications. *Small* **7**, 425–443 (2011).
- Hui, C. *et al.* Core-shell Fe₃O₄@ SiO₂ nanoparticles synthesized with well-dispersed hydrophilic Fe₃O₄ seeds. *Nanoscale* **3**, 701–705 (2011).
- Mirbagheri, R. & Elhamifar, D. Magnetic ethyl-based organosilica supported Schiff-base/indium: A very efficient and highly durable nanocatalyst. *J. Alloys Compd.* **790**, 783–791 (2019).
- Dai, J. *et al.* Yolk-shell Fe₃O₄@ SiO₂@ PMO: Amphiphilic magnetic nanocomposites as an adsorbent and a catalyst with high efficiency and recyclability. *Green Chem.* **19**, 1336–1344 (2017).
- Tudorache, M. *et al.* Highly efficient, easily recoverable, and recyclable re-SiO₂-Fe₃O₄ catalyst for the fragmentation of lignin. *ACS Sustain. Chem. Eng.* **6**, 9606–9618 (2018).
- Shaker, M. & Elhamifar, D. Magnetic Ti-containing phenylene-based mesoporous organosilica: A powerful nanocatalyst with high recoverability. *Colloids Surf. A* **608**, 125603 (2021).
- Shaker, M. & Elhamifar, D. Cu-containing magnetic yolk-shell structured ionic liquid-based organosilica nanocomposite: A powerful catalyst with improved activity. *Compos. Commun.* **24**, 100608 (2020).
- Ghorbani-Vaghei, R., Alavinia, S. & Sarmast, N. Fe₃O₄@ SiO₂@ propyl-ANDSA: A new catalyst for the synthesis of tetrazoloquinazolines. *Appl. Organomet. Chem.* **32**, e4038 (2018).
- Li, W.-P., Liao, P.-Y., Su, C.-H. & Yeh, C.-S. Formation of oligonucleotide-gated silica shell-coated Fe₃O₄-Au core-shell nanotriscap octahedra for magnetically targeted and near-infrared light-responsive theranostic platform. *J. Am. Chem. Soc.* **136**, 10062–10075 (2014).
- Beitollahi, H., Nejad, F. G. & Shakeri, S. GO/Fe₃O₄@ SiO₂ core-shell nanocomposite-modified graphite screen-printed electrode for sensitive and selective electrochemical sensing of dopamine and uric acid. *Anal. Methods* **9**, 5541–5549 (2017).
- Liu, H., Wang, Q. & Zhang, F. Preparation of Fe₃O₄@ SiO₂@ P (AANA-co-AM) composites and their adsorption for Pb (II). *ACS Omega* **5**, 8816–8824 (2020).
- Zhang, L., Liu, B. & Dong, S. Bifunctional nanostructure of magnetic core luminescent shell and its application as solid-state electrochemiluminescence sensor material. *J. Phys. Chem. B* **111**, 10448–10452 (2007).
- Zhou, L., Gao, C. & Xu, W. Robust Fe₃O₄/SiO₂-Pt/Au/Pd magnetic nanocatalysts with multifunctional hyperbranched polyglycerol amplifiers. *Langmuir* **26**, 11217–11225 (2010).

40. Li, W. *et al.* Fabrication of PEI grafted Fe₃O₄/SiO₂/P (GMA-co-EGDMA) nanoparticle anchored palladium nanocatalyst and its application in Sonogashira cross-coupling reactions. *New J. Chem.* **39**, 2925–2934 (2015).
41. Bruzzoniti, M. C. *et al.* MCM41 functionalized with ethylenediaminetriacetic acid for ion-exchange chromatography. *J. Mater. Chem.* **21**, 369–376 (2011).
42. Sardarian, A. R., Inaloo, I. D. & Zangiabadi, M. An Fe₃O₄@SiO₂/Schiff base/Cu (ii) complex as an efficient recyclable magnetic nanocatalyst for selective mono N-arylation of primary O-alkyl thiocarbamates and primary O-alkyl carbamates with aryl halides and arylboronic acids. *New J. Chem.* **43**, 8557–8565 (2019).
43. Dindarloo Inaloo, I., Majnooni, S., Eslahi, H. & Esmaeilpour, M. Nickel (II) nanoparticles immobilized on EDTA-Modified Fe₃O₄@SiO₂ Nanospheres as Efficient and Recyclable Catalysts for Ligand-Free Suzuki-Miyaura Coupling of Aryl Carbamates and Sulfamates. *ACS Omega* **5**, 7406–7417 (2020).
44. Garkoti, C., Shabir, J. & Mozumdar, S. An imidazolium based ionic liquid supported on Fe₃O₄@SiO₂ nanoparticles as an efficient heterogeneous catalyst for N-formylation of amines. *New J. Chem.* **41**, 9291–9298 (2017).
45. Lv, M. *et al.* Magnetically recoverable bifunctional catalysts for the conversion of cellulose to 1, 2-propylene glycol. *ACS Sustain. Chem. Eng.* **8**, 3617–3625 (2020).
46. Wu, Z. *et al.* Brønsted acidic ionic liquid modified magnetic nanoparticle: An efficient and green catalyst for biodiesel production. *Ind. Eng. Chem. Res.* **53**, 3040–3046 (2014).
47. Takaya, J. Catalysis using transition metal complexes featuring main group metal and metalloid compounds as supporting ligands. *Chem. Sci.* **12**, 1964–1981 (2021).
48. Yoo, K. *et al.* Recent organic transformations with silver carbonate as a key external base and oxidant. *Catalysts* **9**, 1032 (2019).
49. Li, M., Wu, W. & Jiang, H. Recent advances in silver-catalyzed transformations of electronically unbiased alkenes and alkynes. *ChemCatChem* **12**, 5034–5050 (2020).
50. Hu, Z., Dong, J. & Xu, X. Silver-catalyzed [3 + 2] cycloaddition of azomethine ylides with isocyanides for imidazole synthesis. *Adv. Synth. Catal.* **359**, 3585–3591 (2017).
51. Wang, H. *et al.* Ag₂CO₃/CA-AA-AmidPhos multifunctional catalysis in the enantioselective 1, 3-dipolar cycloaddition of azomethine ylides. *Org. Lett.* **18**, 404–407 (2016).
52. Kumar, V., Talisman, I. J. & Malhotra, S. V. *Application of Halide Molten Salts as Novel Reaction Media for O-Glycosidic Bond Formation* (Wiley, 2010).
53. Cayuelas, A. *et al.* Cooperative catalysis with coupled chiral induction in 1, 3-dipolar cycloadditions of azomethine ylides. *Chem. Eur. J.* **24**, 8092–8097 (2018).
54. Mirbagheri, R., Elhamifar, D. & Norouzi, M. Propylamine-containing magnetic ethyl-based organosilica with a core-shell structure: An efficient and highly stable nanocatalyst. *New J. Chem.* **42**, 10741–10750 (2018).
55. Dhakshinamoorthy, A., Heidenreich, N., Lenzen, D. & Stock, N. Knoevenagel condensation reaction catalysed by Al-MOFs with CAU-1 and CAU-10-type structures. *CrystEngComm* **19**, 4187–4193 (2017).
56. Sadgar, A. L., Deore, T. S. & Jayaram, R. V. Pickering interfacial catalysis—Knoevenagel condensation in magnesium oxide-stabilized pickering emulsion. *ACS Omega* **5**, 12224–12235 (2020).
57. Elhamifar, D., Kazempoor, S. & Karimi, B. Amine-functionalized ionic liquid-based mesoporous organosilica as a highly efficient nanocatalyst for the Knoevenagel condensation. *Catal. Sci. Technol.* **6**, 4318–4326 (2016).
58. Meng, D., Qiao, Y., Wang, X., Wen, W. & Zhao, S. DABCO-catalyzed Knoevenagel condensation of aldehydes with ethyl cyanoacetate using hydroxy ionic liquid as a promoter. *RSC Adv.* **8**, 30180–30185 (2018).
59. Gawande, M. B. & Jayaram, R. V. A novel catalyst for the Knoevenagel condensation of aldehydes with malononitrile and ethyl cyanoacetate under solvent free conditions. *Catal. Commun.* **7**, 931–935 (2006).
60. Senapati, K. K., Borgohain, C. & Phukan, P. Synthesis of highly stable CoFe₂O₄ nanoparticles and their use as magnetically separable catalyst for Knoevenagel reaction in aqueous medium. *J. Mol. Catal. A* **339**, 24–31 (2011).
61. Li, T., Zhang, W., Chen, W., Miras, H. N. & Song, Y.-F. Layered double hydroxide anchored ionic liquids as amphiphilic heterogeneous catalysts for the Knoevenagel condensation reaction. *Dalton Trans.* **47**, 3059–3067 (2018).
62. Heravi, M. M., Tehrani, M. H., Bakhtiari, K. & Oskooie, H. A. A practical Knoevenagel condensation catalysed by imidazole. *J. Chem. Res.* **2006**, 561–562 (2006).
63. Cabello, J. A., Campelo, J. M., Garcia, A., Luna, D. & Marinas, J. M. Knoevenagel condensation in the heterogeneous phase using aluminum phosphate-aluminum oxide as a new catalyst. *J. Org. Chem.* **49**, 5195–5197 (1984).
64. Kolahdoozan, M., Kalbasi, R. J., Shahzeidi, Z. S. & Zamani, F. Knoevenagel condensation of aldehydes with ethyl cyanoacetate in water catalyzed by P4VP/Al₂O₃-SiO₂. *J. Chem.* **2013**, 1–8 (2013).
65. Roso, M., Boaretti, C., Bonora, R., Modesti, M. & Lorenzetti, A. Nanostructured active media for volatile organic compounds abatement: The synergy of graphene oxide and semiconductor coupling. *Ind. Eng. Chem. Res.* **57**, 16635–16644 (2018).
66. Song, Y. *et al.* Synthesis, characterization and visible-light photocatalytic performance of Ag₂CO₃ modified by graphene-oxide. *J. Alloys Compd.* **592**, 258–265 (2014).
67. Guo, S. *et al.* Controllable synthesis porous Ag₂CO₃ nanorods for efficient photocatalysis. *Nanoscale Res. Lett.* **10**, 1–8 (2015).
68. Tietze, L. F. & Beifuss, U. The Knoevenagel reaction. *Compr. Org. Synth.* **2**, 341–394 (1992).
69. Schneider, E. M., Zeltner, M., Kränzlin, N., Grass, R. N. & Stark, W. J. Base-free Knoevenagel condensation catalyzed by copper metal surfaces. *Chem. Commun.* **51**, 10695–10698 (2015).
70. Zhang, Q., Ma, X.-M., Wei, H.-X., Zhao, X. & Luo, J. Covalently anchored tertiary amine functionalized ionic liquid on silica coated nano-Fe₃O₄ as a novel, efficient and magnetically recoverable catalyst for the unsymmetrical Hantzsch reaction and Knoevenagel condensation. *RSC Adv.* **7**, 53861–53870 (2017).
71. Zhao, S., Meng, D., Wei, L., Qiao, Y. & Xi, F. Novel DBU-based hydroxyl ionic liquid for efficient Knoevenagel reaction in water. *Green Chem. Lett. Rev.* **12**, 271–277 (2019).
72. Li, P., Liu, Y., Ma, N. & Zhang, W. L-Lysine functionalized polyacrylonitrile fiber: A green and efficient catalyst for Knoevenagel condensation in water. *Catal. Lett.* **148**, 813–823 (2018).
73. Patel, D., Vithalani, R. & Modi, C. K. Highly efficient FeNP-embedded hybrid bifunctional reduced graphene oxide for Knoevenagel condensation with active methylene compounds. *New J. Chem.* **44**, 2868–2881 (2020).
74. Ghosh, M. K., Jain, K., Khan, S., Das, K. & Ghorai, T. K. New dual-functional and reusable bimetallic Y₂ZnO₄ nanocatalyst for organic transformation under microwave/green conditions. *ACS Omega* **5**, 4973–4981 (2020).
75. Kim, H.-C., Huh, S., Kim, S.-J. & Kim, Y. Selective carbon dioxide sorption and heterogeneous catalysis by a new 3D Zn-MOF with nitrogen-rich 1D channels. *Sci. Rep.* **7**, 1–12 (2017).
76. Song, X. *et al.* Three amino-functionalized alkaline earth metal-organic frameworks as catalysts for Knoevenagel condensation. *ChemistrySelect* **5**, 11510–11516 (2020).
77. Mondal, R. K. *et al.* Polymer immobilized [Mg@PS-anthra] complex: An efficient recyclable heterogeneous catalyst for the incorporation of carbon dioxide into oxiranes at atmospheric pressure and Knoevenagel condensation reaction under solvent free condition. *J. Organomet. Chem.* **880**, 322–332 (2019).

Acknowledgements

The authors thank the Yasouj University and the Iran National Science Foundation (INSF) for supporting this work.

Author contributions

F.K.: Investigation, Formal analysis. D.E.: Conceptualization, Writing—Review & Editing, Supervision, Visualization. M.S.: Writing—Original Draft, Resources, Formal analysis.

Competing interests

The authors declare no competing interests.

Additional information

Correspondence and requests for materials should be addressed to D.E.

Reprints and permissions information is available at www.nature.com/reprints.

Publisher's note Springer Nature remains neutral with regard to jurisdictional claims in published maps and institutional affiliations.



Open Access This article is licensed under a Creative Commons Attribution 4.0 International License, which permits use, sharing, adaptation, distribution and reproduction in any medium or format, as long as you give appropriate credit to the original author(s) and the source, provide a link to the Creative Commons licence, and indicate if changes were made. The images or other third party material in this article are included in the article's Creative Commons licence, unless indicated otherwise in a credit line to the material. If material is not included in the article's Creative Commons licence and your intended use is not permitted by statutory regulation or exceeds the permitted use, you will need to obtain permission directly from the copyright holder. To view a copy of this licence, visit <http://creativecommons.org/licenses/by/4.0/>.

© The Author(s) 2021